Available online at www.sciencedirect.com
SCIENCE DIRECT®
ELSEVIER
Advances in Applied Mathematics 32 (2004) 681–697
ADVANCES IN Applied Mathematics
www.elsevier.com/locate/yaama

An improved exact filtered backprojection algorithm for spiral computed tomography ☆

Alexander Katsevich

Department of Mathematics, University of Central Florida, Orlando, FL 32816-1364, USA

Received 17 September 2002; accepted 5 May 2003

Abstract

Proposed is a theoretically exact formula for inversion of data obtained by a spiral computed tomography scan with a two-dimensional detector array. The detector array is supposed to be of limited extent in the axial direction. The main property of the formula is that it can be implemented in a truly filtered backprojection fashion. First, one performs shift-invariant filtering of a derivative of the cone beam projections, and, second, the result is back-projected in order to form an image. Compared with an earlier reconstruction algorithm proposed by the author, the new one is two times faster, requires a smaller detector array, and does not impose restrictions on how big the patient is inside the gantry. Results of numerical experiments are presented.

Keywords: Cone-beam; Spiral tomography; Theoretically exact reconstruction; Filtered back-projection algorithm

1. Introduction

In this paper we continue to develop an approach for inverting the spiral cone beam data, that was proposed earlier by the author in [Kat01,Kat02b]. In these papers the first theoretically exact inversion formula of the filtered backprojection (FBP) type was proposed. The formula can be numerically implemented in two steps. First, one performs shift-invariant filtering of a derivative of the cone beam projections, and, second, the result is back-projected in order to form an image. The price to pay for this efficient structure is that the algorithm requires an array wider than the theoretically minimum one. Also, the

☆ This research was supported in part by NSF grant DMS-0104033.
E-mail address: akatsevi@pegasus.cc.ucf.edu.

0196-8858/$ – see front matter
doi:10.1016/S0196-8858(03)00099-X

algorithm is applicable if radius of support of the patient inside the gantry is not too big (not greater than $\approx 0.62 \times$ radius of gantry).

In the present paper we propose an improved algorithm which is still theoretically exact and of the FBP type, but has fewer drawbacks. First, in the new algorithm there is no restriction on the size of the patient as long as he/she fits inside the gantry. Second, the new algorithm requires a smaller detector array than the old one. For example, if r and R denote radius of the patient and radius of the gantry, respectively, then in the case $r/R = 0.5$ the area of the detector array required for the old algorithm is $1.93\, A_{\min}$, and for the new one—$1.21\, A_{\min}$. Here $A_{\min}$ denotes the theoretically minimal area. Third, the new algorithm is two times faster than the old one.

In Section 2 we derive the new inversion formula. In Section 3 its proof is given, and in Section 4 we show that the resulting algorithm is of the FBP type and present the results of three numerical experiments.

2. Inversion formulas

First, we introduce the necessary notations. Let

$$C := \left\{ y \in \mathbb{R}^3 \colon\ y_1 = R\cos(s),\ y_2 = R\sin(s),\ y_3 = s(h/2\pi),\ s \in \mathbb{R} \right\}, \quad h > 0, \tag{2.1}$$

be a spiral, U—an open cylinder strictly inside the spiral

$$U := \left\{ x \in \mathbb{R}^3 \colon\ x_1^2 + x_2^2 < r^2 \right\}, \quad 0 < r < R, \tag{2.2}$$

S^2 is the unit sphere in $\mathbb{R}^3$, and

$$D_f(y, \Theta) := \int_0^\infty f(y + \Theta t)\, \mathrm{d}t, \quad \Theta \in S^2, \tag{2.3}$$

$$\beta(s, x) := \frac{x - y(s)}{|x - y(s)|}, \quad x \in U,\ s \in I,$$

$$\Pi(x, \xi) := \left\{ y \in \mathbb{R}^3 \colon\ (y - x) \cdot \xi = 0 \right\}. \tag{2.4}$$

Here $D_f(y, \beta)$ is the cone beam transform of f. Given $(x, \xi) \in U \times (\mathbb{R}^3 \setminus 0)$, let $y(s_j)$, $s_j = s_j(\xi, \xi \cdot x)$, $j = 1, 2, \ldots$, denote the points of intersection of $\Pi(x, \xi)$ with C. Also, $\dot{y}(s) := \mathrm{d}y/\mathrm{d}s$ and j_3 is the unit vector along the x_3-axis.

Let $s = s_b(x)$ and $s = s_t(x)$ denote values of the parameter corresponding to the endpoints of the PI segment containing x (see [D$^+$97,DNK00,Kat02b]). We call $I_{\mathrm{PI}}(x) := [s_b(x), s_t(x)]$ the PI parametric interval. The part of the spiral corresponding to $I_{\mathrm{PI}}(x)$ is denoted $C_{\mathrm{PI}}(x)$.

Choose any $\psi \in C^\infty([0, 2\pi])$ with the properties

$$\psi(0) = 0, \qquad 0 < \psi'(t) < 1,\ t \in [0, 2\pi]. \tag{2.5}$$

Suppose s_0, s_1, and s_2 are related by

$$s_1 = \begin{cases} \psi(s_2 - s_0) + s_0, & s_0 \leqslant s_2 < s_0 + 2\pi, \\ \psi(s_0 - s_2) + s_2, & s_0 - 2\pi < s_2 < s_0. \end{cases} \tag{2.6}$$

Since $\psi(0) = 0$, $s_1 = s_1(s_0, s_2)$ is a continuous function of s_0 and s_2. (2.5) and (2.6) imply $s_1 \neq s_2$ unless $s_0 = s_1 = s_2$. In order to avoid unnecessary complications, we will assume in what follows

$$\psi'(0) = 0.5, \quad \psi^{(2k+1)}(0) = 0,\ k \geqslant 1. \tag{2.7}$$

If (2.7) holds, then $s_1 = s_1(s_0, s_2)$ is a C^∞ function of s_0 and s_2. Conditions (2.5) and (2.7) are very easy to satisfy. One can take, for example, $\psi(t) = t/2$, and this leads to

$$s_1 = (s_0 + s_2)/2, \quad s_0 - 2\pi < s_2 < s_0 + 2\pi. \tag{2.8}$$

Denote also

$$\begin{aligned} u(s_0, s_2) &= \frac{(y(s_1) - y(s_0)) \times (y(s_2) - y(s_0))}{|(y(s_1) - y(s_0)) \times (y(s_2) - y(s_0))|} \operatorname{sgn}(s_2 - s_0), \quad 0 < |s_2 - s_0| < 2\pi, \\ u(s_0, s_2) &= \frac{\dot{y}(s_0) \times \ddot{y}(s_0)}{|\dot{y}(s_0) \times \ddot{y}(s_0)|}, \quad s_2 = s_0. \end{aligned} \tag{2.9}$$

Using (2.5), (2.6), and the property that $s_1 - s_0$ and $s_2 - s_0$ are always of the same sign, we find

$$u(s_0, s_2) = \frac{\dot{y}(s_0) \times \ddot{y}(s_0) + O(s_2 - s_0)}{|\dot{y}(s_0) \times \ddot{y}(s_0) + O(s_2 - s_0)|}, \quad s_2 \to s_0. \tag{2.10}$$

Hence, $u(s_0, s_2)$ is a C^∞ vector function of its arguments. Also $u(s_0, s_2) \cdot j_3 > 0$. Indeed, assume without loss of generality that $s_0 = 0$ and consider the case $0 < s_1 < s_2 < 2\pi$. Using (2.1),

$$\begin{aligned} u(s_0, s_2) \cdot j_3 &= \frac{R^2}{c}\big[\big(\cos(s_1) - 1\big)\sin(s_2) - \sin(s_1)\big(\cos(s_2) - 1\big)\big] \\ &= \frac{4R^2}{c} \sin(s_1/2) \sin(s_2/2) \sin\big((s_2 - s_1)/2\big) > 0, \end{aligned} \tag{2.11}$$

where $c > 0$ is the denominator in (2.9). The cases $-2\pi < s_2 < s_1 < 0$ and $s_1 = s_2 = 0$ can be considered similarly.

Fix $x \in U$ and $s_0 \in I_{\mathrm{PI}}(x)$. Find $s_2 \in I_{\mathrm{PI}}(x)$ such that the plane through $y(s_0)$, $y(s_2)$, and $y(s_1(s_0, s_2))$ contains x. More precisely, we have to solve for s_2 the following equation:

$$\big(x - y(s_0)\big) \cdot u(s_0, s_2) = 0, \quad s_2 \in I_{\mathrm{PI}}(x). \tag{2.12}$$

It is shown below (see (3.5) and the argument around it) that such s_2 exists, is unique, and depends smoothly on s_0. Therefore, this construction defines $s_2 := s_2(s_0, x)$ and, consequently, $u(s_0, x) := u(s_0, s_2(s_0, x))$. Our main result is the following theorem.

Theorem 1. *For $f \in C_0^\infty(U)$ one has*

$$f(x) = -\frac{1}{2\pi^2} \int\limits_{I_{\mathrm{PI}}(x)} \frac{1}{|x - y(s)|} \int\limits_0^{2\pi} \frac{\partial}{\partial q} D_f\big(y(q), \Theta(s, x, \gamma)\big)\Big|_{q=s} \frac{\mathrm{d}\gamma}{\sin\gamma}\,\mathrm{d}s, \tag{2.13}$$

where $e(s, x) := \beta(s, x) \times u(s, x)$ and $\Theta(s, x, \gamma) := \cos\gamma\beta(s, x) + \sin\gamma e(s, x)$.

Comparing (2.13) with the results of [Kat01,Kat02b] we see that the reconstruction formula of [Kat01,Kat02b] consists of two integrals, each of which is analogous to (2.13). Therefore, the algorithm proposed in this paper is two times faster than the older one.

Integrating by parts with respect to s in (2.13) we obtain an inversion formula in which all the derivatives are performed with respect to the angular variables (see [Kat02a] for details):

$$\begin{aligned} f(x) = -\frac{1}{2\pi^2} \Bigg\{ & \left[\frac{1}{|x - y(s)|} \int\limits_0^{2\pi} D_f\big(y(s), \Theta(s, x, \gamma)\big) \frac{\mathrm{d}\gamma}{\sin\gamma} \right] \Bigg|_{s=s_b(x)}^{s=s_t(x)} \\ & - \int\limits_{I_{\mathrm{PI}}(x)} \left(\frac{\partial}{\partial s} \frac{1}{|x - y(s)|} \right) \int\limits_0^{2\pi} D_f\big(y(s), \Theta(s, x, \gamma)\big) \frac{\mathrm{d}\gamma}{\sin\gamma}\,\mathrm{d}s \\ & - \int\limits_{I_{\mathrm{PI}}(x)} \frac{\beta_s'(s, x) \cdot u(s, x)}{|x - y(s)|} \int\limits_0^{2\pi} (\nabla_{u(s,x)} D_f)\big(y(s), \Theta(s, x, \gamma)\big) \cot(\gamma)\,\mathrm{d}\gamma\,\mathrm{d}s \\ & - \int\limits_{I_{\mathrm{PI}}(x)} \frac{e_s'(s, x) \cdot u(s, x)}{|x - y(s)|} \int\limits_0^{2\pi} (\nabla_{u(s,x)} D_f)\big(y(s), \Theta(s, x, \gamma)\big)\,\mathrm{d}\gamma\,\mathrm{d}s \\ & - \int\limits_{I_{\mathrm{PI}}(x)} \frac{\beta_s'(s, x) \cdot e(s, x)}{|x - y(s)|} \int\limits_0^{2\pi} \left(\frac{\partial}{\partial\gamma} D_f\big(y(s), \Theta(s, x, \gamma)\big) \right) \frac{\mathrm{d}\gamma}{\sin\gamma}\,\mathrm{d}s \Bigg\}. \end{aligned} \tag{2.14}$$

Here $\beta_s' = \partial\beta/\partial s$, $e_s' = \partial e/\partial s$, and $\nabla_u D_f$ denotes the derivative of D_f with respect to the angular variables along the direction u:

$$(\nabla_u D_f)\big(y(s), \Theta\big) = \frac{\partial}{\partial t} D_f\big(y(s), \sqrt{1 - t^2}\,\Theta + tu\big)\big|_{t=0}, \quad \Theta \in u^\perp. \tag{2.15}$$

3. Proof of Theorem 1

Let $x \in U$ be fixed. It is clear that any plane through x intersects $C_{\mathrm{PI}}(x)$ at least at one point. Introduce the following sets:

$$\begin{aligned}
\mathrm{Crit}(x) &= \big\{\xi \in \mathbb{R}^3 \setminus 0\colon\ \Pi(x,\xi) \text{ contains } y\big(s_b(x)\big),\ y\big(s_t(x)\big) \text{ or} \\
&\qquad\qquad \Pi(x,\xi) \text{ is tangent to } C_{\mathrm{PI}}(x)\big\} \cup \{0\}, \\
\Xi_1(x) &= \big\{\xi \in \mathbb{R}^3\colon\ \xi \notin \mathrm{Crit}(x) \text{ and } \Pi(x,\xi) \cap C_{\mathrm{PI}}(x) \text{ contains one point}\big\}, \\
\Xi_3(x) &= \mathbb{R}^3 \setminus \big\{\Xi_1(x) \cup \mathrm{Crit}(x)\big\}, \\
\Xi_\psi(x) &= \big\{\xi \in \mathbb{R}^3\colon\ \xi = \lambda\, u(s,x),\ s \in I_{\mathrm{PI}}(x),\ \lambda \in \mathbb{R}\big\}.
\end{aligned} \tag{3.1}$$

Recall that $u(s,x)$ was defined above Theorem 1. By construction, the sets $\mathrm{Crit}(x)$, $\Xi_{1,3}(x)$ are pairwise disjoint, their union is all of $\mathbb{R}^3$, $\mathrm{Crit}(x)$ and $\Xi_\psi(x)$ have Lebesgue measure zero, and $\Xi_{1,3}(x)$ are open.

Similarly to [Kat02b, (2.14)–(2.22)] we obtain that the right-hand side of (2.13) is equal to

$$\frac{1}{(2\pi)^3} \int_{\mathbb{R}^3} B(x,\xi)\, \tilde{f}(\xi) e^{-i\xi\cdot x}\, \mathrm{d}\xi, \tag{3.2}$$

where $B(x,\xi) \in L^\infty(\mathbb{R}^3)$ and

$$B(x,\xi) = \sum_{s_j \in I_{\mathrm{PI}}(x)} \mathrm{sgn}\big(\xi \cdot \dot{y}(s_j)\big)\, \mathrm{sgn}\big(\xi \cdot e(s_j,x)\big), \quad \xi \notin \mathrm{Crit}(x) \cup \Xi_\psi(x). \tag{3.3}$$

Recall that $s_j = s_j(\xi, \xi\cdot x)$, $j = 1,2,\ldots$, denote parameter values corresponding to points of intersection of the plane $\Pi(x,\xi)$ with the spiral and are found by solving $\xi \cdot (x - y(s)) = 0$. Here we have used that $\xi \notin \mathrm{Crit}(x) \cup \Xi_\psi(x)$ and $\xi \cdot (x - y(s_j)) = 0$ imply $\xi \cdot \dot{y}(s_j) \neq 0$ and $\xi \cdot e(s_j,x) \neq 0$. Indeed, if $\xi \cdot \dot{y}(s_j) = 0$, then $\Pi(x,\xi)$ is tangent to $C_{\mathrm{PI}}(x)$ at $y(s_j)$ and $\xi \in \mathrm{Crit}(x)$. If $\xi \cdot e(s_j,x) = 0$, then together with $\xi \cdot \beta(s_j,x) = 0$ this implies $\xi \in \Xi_\psi(x)$. In both cases we get a contradiction. This argument implies also that $B(x,\xi)$ is locally constant in a neighborhood of any $\xi \notin \mathrm{Crit}(x) \cup \Xi_\psi(x)$.

It follows from (3.3) that in order to finish the proof we have to show that $B(x,\xi) = 1$ for almost all $\xi \in \mathbb{R}^3$.

Suppose first that the X-ray source is fixed at $y(s_0)$ for some $s_0 \in I_{\mathrm{PI}}(x)$. Similarly to [Kat02b], project stereographically the upper and lower turns of the spiral onto the detector plane. Since the detector array rotates together with the source, the detector plane depends on s_0 and is denoted $DP(s_0)$. It is assumed that $DP(s_0)$ is parallel to the axis of the spiral and is tangent to the cylinder $y_1^2 + y_2^2 = R^2$ (cf. (2.1)) at the point opposite to the source. Thus, the distance between $y(s_0)$ and the detector plane is $2R$. Introduce coordinates in the detector plane as follows. Let the d_1-axis be perpendicular to the axis of the spiral, and the d_2-axis be parallel to it. This gives the following parametric curves:

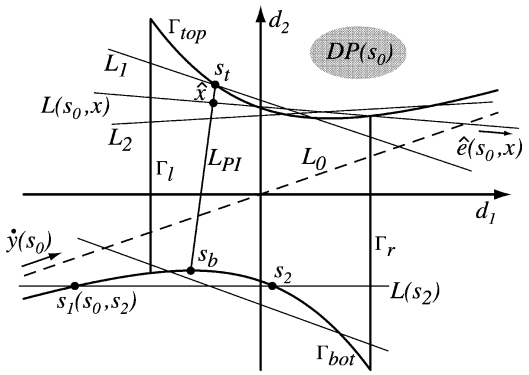

Fig. 1. Some of the lines from the family $L(s_2)$ are shown. $L(s_0, x)$ denotes the line in the family which contains $\hat{x}$.

$$d_1(s) = 2R\frac{\sin(s-s_0)}{1-\cos(s-s_0)}, \qquad d_2(s) = \frac{h}{\pi}\frac{s-s_0}{1-\cos(s-s_0)},$$
$$\Delta \leqslant s - s_0 \leqslant 2\pi - \Delta \quad \text{or} \quad \Delta - 2\pi \leqslant s - s_0 \leqslant -\Delta, \tag{3.4}$$

where Δ is determined by the radius of U: $\Delta = 2\cos^{-1}(r/R)$ (cf. (2.2)). The top and bottom curves are denoted Γ_{top} and Γ_{bot}, respectively, and $\hat{x}$ denotes the projection of x (see Fig. 1). Γ_l and Γ_r are sections of the boundary of the projection of U onto $DP(s_0)$ that are located between Γ_{bot} and Γ_{top}. Since $s_0 \in I_{\text{PI}}(x)$ and $x \in U$, $\hat{x}$ is projected into the region bounded by Γ_{top}, Γ_{bot}, Γ_l, and Γ_r. L_0 denotes the intersection of the plane containing $y(s_0)$ and parallel to $\dot{y}(s_0)$, $\ddot{y}(s_0)$, with $DP(s_0)$. L_{PI} is the projection of the PI segment of x onto $DP(s_0)$. See [Kat02b] for a short discussion of the properties of Γ_{top}, Γ_{bot}, L_0 and L_{PI}.

Consider a one-parametric family of planes $\Pi(s_2)$ passing through $y(s_0)$, $y(s_2)$, and $y(s_1(s_0, s_2))$. Intersections of these planes with the detector plane $DP(s_0)$ produces a family of lines $L(s_2)$ (see Fig. 1). By construction, either $s_0 < s_1 < s_2$, or $s_2 < s_1 < s_0$, or $s_0 = s_1 = s_2$. Therefore, if $s_0 < s_1 < s_2$, $L(s_2)$ intersects Γ_{top} at two points. If $s_2 < s_1 < s_0$, $L(s_2)$ intersects Γ_{bot} at two points. And, by continuity, $L(s_2) = L_0$ if $s_0 = s_1 = s_2$. Suppose, for example, that $\hat{x}$ is located above L_0. Selecting $s_2 = s_t(x)$, it is clear that $L(s_2 = s_t(x))$ passes above $\hat{x}$ (see line L_1 in Fig. 1). On the other hand, taking s_2 sufficiently close to s_0, $s_2 > s_0$, $L_2(s_2)$ will pass below $\hat{x}$ (see line L_2 in Fig. 1). Therefore, there exists at least one $s_2 > s_0$ such that $\hat{x} \in L(s_2)$. This line is denoted $L(s_0, x)$. Suppose there are two values s_2, s_2', $s_0 < s_2' < s_2 < s_t(x)$ such that $\hat{x} \in L(s_2)$ and $\hat{x} \in L(s_2')$. Since $\hat{x}$ is below Γ_{top}, this implies

$$s_0 < s_1 < s_1' < s_2' < s_2, \quad s_1 := s_1(s_0, s_2), \quad s_1' := s_1(s_0, s_2'). \tag{3.5}$$

From (2.6), $\partial s_1/\partial s_2 = \psi'(s_2 - s_0) > 0$, that is $s_2 > s_2'$ implies $s_1 > s_1'$, and this contradicts (3.5). Hence, there exists a unique s_2, $s_0 < s_2 < s_t(x)$, such that $x \in \Pi(s_2)$. The case when $\hat{x}$ appears below L_0 can be considered similarly. If $\hat{x} \in L_0$, then the unique solution is $s_2 = s_0$.

To prove that $s_2 = s_2(s_0, x)$ depends smoothly on s_0 we first consider the case when s_0 is such that $s_2(s_0, x)$ and s_0 are close. According to the preceding discussion this happens when $s_0 \to \check{s}(x)$, where $\check{s}(x) \in I_{\mathrm{PI}}(x)$ is the unique value such that the plane through $y(\check{s}(x))$ and parallel to $\dot{y}(\check{s}(x)), \ddot{y}(\check{s}(x))$ contains x. It is easily seen that such $\check{s}(x)$ exists and is unique. To simplify the notation, assume without loss of generality that $\check{s}(x) = 0$. Thus,

$$x = y(0) + a\dot{y}(0) + b\ddot{y}(0), \quad b > 0. \tag{3.6}$$

The condition $b > 0$ follows from $x \in U$. Taking into account the terms of the first order of smallness and using (2.7), we find analogously to (2.10)

$$u(s_0, s_2) = \frac{[\dot{y}(s_0) \times \ddot{y}(s_0)] + [\dot{y}(s_0) \times \dddot{y}(s_0)]\frac{s_2 - s_0}{2} + O((s_2 - s_0)^2)}{|[\dot{y}(s_0) \times \ddot{y}(s_0)] + [\dot{y}(s_0) \times \dddot{y}(s_0)]\frac{s_2 - s_0}{2} + O((s_2 - s_0)^2)|}, \quad s_2 \to s_0. \tag{3.7}$$

Substituting (3.6) and (3.7) into (2.12), implicitly differentiating the resulting equation with respect to s_0, and then setting $s_0 = 0$ gives

$$\left\{b\ddot{y}(0) \cdot \left(\dot{y}(0) \times \dddot{y}(0)\right)\right\}\left[1 + \frac{(\partial s_2/\partial s_0) - 1}{2}\right] = 0. \tag{3.8}$$

Since the expression in braces is not zero, we find

$$\left.\frac{\partial s_2(s_0, x)}{\partial s_0}\right|_{s_0 = \check{s}(x)} = -1. \tag{3.9}$$

Suppose now $s_0 \in (s_b(x), s_t(x))$, $s_0 \neq \check{s}(x)$. Instead of solving (2.12) for s_2, we can find the appropriate line $L(s_2)$ in Fig. 1 which contains $\hat{x}$. Let $(\hat{x}_1(s_0), \hat{x}_2(s_0))$ be the coordinates of $\hat{x}$ on the detector plane $DP(s_0)$. Obviously, these coordinates depend smoothly on s_0. Consider, for example, the case when $\hat{x}$ appears above L_0. Then $s_0 < s_1 < s_2$. The equation for s_2 is

$$\frac{\hat{x}_2(s_0) - d_2(s_2 - s_0)}{\hat{x}_2(s_0) - d_2(s_1 - s_0)} = \frac{\hat{x}_1(s_0) - d_1(s_2 - s_0)}{\hat{x}_1(s_0) - d_1(s_1 - s_0)}. \tag{3.10}$$

To simplify the notation, after all the differentiations have been carried out the dependence of $\hat{x}_{1,2}$ on s_0 is dropped and it is assumed without loss of generality that $s_0 = 0$. Multiplying (3.10) out, taking into account $s_1 - s_0 = \psi(s_2 - s_0)$, and differentiating with respect to s_0, we obtain an equation in which $\partial s_2/\partial s_0$ is multiplied by

$$\begin{aligned}\kappa := {} & d_1'(s_2)\big(\hat{x}_2 - d_2(s_1)\big) + d_2'(s_1)\psi'(s_2)\big(\hat{x}_1 - d_1(s_2)\big) \\ & - d_2'(s_2)\big(w\hat{x}_1 - d_1(s_1)\big) - d_1'(s_1)\psi'(s_2)\big(\hat{x}_2 - d_2(s_2)\big).\end{aligned} \tag{3.11}$$

In view of the implicit function theorem we have to show $\kappa \neq 0$. Dividing by $\hat{x}_1 - d_1(s_1) \neq 0$ and using (3.10) transforms (3.11) to

$$d_1'(s_2)\left[\frac{\hat{x}_2 - d_2(s_2)}{\hat{x}_1 - d_1(s_2)} - \frac{d_2'(s_2)}{d_1'(s_2)}\right] + \psi'(s_2)d_1'(s_1)\frac{\hat{x}_1 - d_1(s_2)}{\hat{x}_1 - d_1(s_1)}\left[\frac{d_2'(s_1)}{d_1'(s_1)} - \frac{\hat{x}_2 - d_2(s_2)}{\hat{x}_1 - d_1(s_2)}\right]. \tag{3.12}$$

Interpreting the ratios in brackets in (3.12) as slopes, we see that the two expressions in brackets are positive (cf. Fig. 1). Using that $d_1'(s_{1,2}) < 0$, $\psi' > 0$, and $\hat{x}_1 < d_1(s_{1,2})$ (again cf. Fig. 1), we prove $\kappa \neq 0$. κ remains bounded away from zero even if $s_0 \to s_b(x)$. In this case $\hat{x} \to \Gamma_{\text{top}}$ and, in the limit $\hat{x} = (d_1(s_2), d_2(s_2))$, where $s_2 = s_t(x)$, (3.12) becomes

$$d_1'(s_2)\left[\frac{d_2(s_2) - d_2(s_1)}{d_1(s_2) - d_1(s_1)} - \frac{d_2'(s_2)}{d_1'(s_2)}\right] < 0, \tag{3.13}$$

where we have used (3.10). The case when $\hat{x}$ appears below L_0 can be treated similarly.

Consider various lines through $\hat{x}$ (see Fig. 2). L_{tan} denotes the line through $\hat{x}$ and tangent to either Γ_{top} if $\hat{x}$ is above L_0, or Γ_{bot} if $\hat{x}$ is below L_0. In both cases the point of tangency should fall inside the PI-parametric interval and, therefore, is unique. The corresponding parameter value is denoted s_{tan}. If $\hat{x} \in L_0$, by continuity $L_{\text{tan}} = L_0$. L_0' is the line through $\hat{x}$ and parallel to L_0. Finally, $L(x,\xi)$ is the intersection of $\Pi(x,\xi) \ni y(s_0)$ with the detector plane. Clearly, there is one-to-one correspondence between the planes $\Pi(x,\xi)$, where ξ satisfies $\xi \cdot (x - y(s_0)) = 0$, and the lines $L(x,\xi)$. The lines L_{PI}, L_{tan}, and L_0' split the detector plane into three conical regions: D_j, $j = 1,2,3$. If $\hat{x} \in L_0$, then $L_{\text{tan}} = L_0$ and D_2 collapses into an empty set. If $L(x,\xi) \subset D_1$, $\Pi(x,\xi) \cap C_{\text{PI}}(x)$ contains only one point—$y(s_0)$. If $L(x,\xi) \subset D_2$, there are three points of intersection of $\Pi(x,\xi)$ with $C_{\text{PI}}(x)$. If $\hat{x}$ is above L_0, they correspond to values of the parameter $s = a, b, c$ that satisfy $a = s_0 < b < c < s_t(x)$. Recall that in this region the slope of $L(x,\xi)$ is smaller than that of L_0. If $\hat{x}$ is below L_0 the situation is essentially the same. The only difference

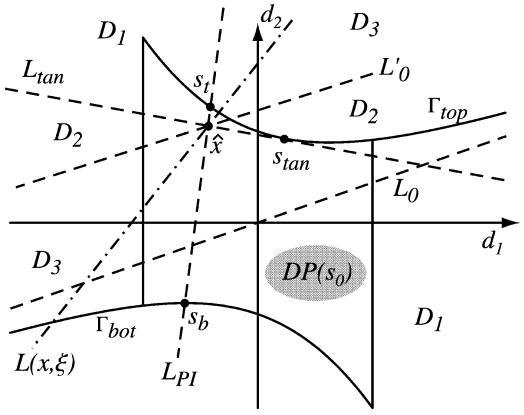

Fig. 2. Detector plane with various lines through $\hat{x}$ shown.

is that $L(x,\xi)\subset D_2$ implies that parameter values at the three points of intersection of $\Pi(x,\xi)$ with $C_{\mathrm{PI}}(x)$ satisfy $s_b<a<b<c=s_0$. If $L(x,\xi)\subset D_3$ (an example of such a line is shown in Fig. 2), then again there are three points of intersection of $\Pi(x,\xi)$ with $C_{\mathrm{PI}}(x)$, and $s_b(x)<a<b=s_0<c<s_t(x)$. This argument shows that if $\xi\in\Xi_1$ (i.e., when $C_{\mathrm{PI}}(x)\cap\Pi(x,\xi)$ consists of one point), then $L(x,\xi)\subset D_1$. If $\xi\in\Xi_3$, then $C_{\mathrm{PI}}(x)\cap\Pi(x,\xi)$ consists of precisely three points and $L(x,\xi)\subset D_2$ or D_3.

In order to compute the value of the sum in (3.3) we need a simplifying argument. Let $\hat{\xi}$ be a nonzero vector in the detector plane $DP(s_0)$ perpendicular to $L(x,\xi)$ and pointing into the same half-space as ξ, that is $\xi\cdot\hat{\xi}>0$. Fix any nonzero vector $e\in\mathbb{R}^3$ perpendicular to $\beta(s_0,x)$, and let L be the line in the intersection of $\Pi(x,\beta(s_0,x)\times e)$ with the detector plane. Analogously, $\hat{e}$ denotes a vector in the detector plane parallel to L and with the property $e\cdot\hat{e}>0$. Similarly to [Kat02b, (2.26)–(2.29)], it is easily seen that

$$\operatorname{sgn}\bigl(\xi\cdot\dot{y}(s_0)\bigr)\operatorname{sgn}\bigl(\xi\cdot e(s_0,x)\bigr)=\operatorname{sgn}\bigl(\hat{\xi}\cdot\dot{y}(s_0)\bigr)\operatorname{sgn}\bigl(\hat{\xi}\cdot\hat{e}(s_0,x)\bigr). \tag{3.14}$$

For convenience, vectors $\dot{y}(s_0)$ and $\hat{e}(s_0,x)$ are shown in Fig. 1. Similarly to [Kat02b] we conclude that $\hat{e}(s_0,x)$ should point to the right, as is shown in Fig. 1. Note that if $\hat{x}\in L_0$, then $L(s_0,x)=L_0$, $\hat{e}(s_0,x)$ and $\dot{y}(s_0)$ are parallel and point in the same direction.

To compute $B(x,\xi)$ we have to consider several cases.

I. $\xi\in\Xi_1(x)$. Since in this case $\Pi(x,\xi)\cap C_{\mathrm{PI}}(x)$ consists of only one point, say $y(s_0)$, $L(x,\xi)\subset D_1$ and $\operatorname{sgn}(\hat{\xi}\cdot\hat{e}(s_0,x))=\operatorname{sgn}(\hat{\xi}\cdot\dot{y}(s_0))$. Hence, from (3.3) and (3.14):

$$B(x,\xi)=\operatorname{sgn}\bigl(\xi\cdot\dot{y}(s_0)\bigr)\operatorname{sgn}\bigl(\xi\cdot e(s_0,x)\bigr)=1,\quad \xi\in\Xi_1(x). \tag{3.15}$$

II. $\xi\in\Xi_3(x)\setminus\Xi_\psi(x)$. In this case there are three points in $\Pi(x,\xi)\cap C_{\mathrm{PI}}(x)$ corresponding to $s_b(x)<a<b<c<s_t(x)$.

II.1. Consider the detector plane $DP(a)$, where a is the smallest value of the parameter among the three points. Since $y(a)$ is the lowest point of intersection and there are two more points in $\Pi(x,\xi)\cap C_{\mathrm{PI}}(x)$, the line $L(x,\xi)$ intersects the part of Γ_{top} corresponding to $a<s<s_t(x)$ at two points (see Fig. 3).

II.1.a. If $c<s_2(a,x)$, then $L(x,\xi)$ passes between $L(a,x)$ and $L_{\tan}$. This case is illustrated by Fig. 3. Consequently,

$$\operatorname{sgn}\bigl(\hat{\xi}\cdot\dot{y}(a)\bigr)=\operatorname{sgn}\bigl(\hat{\xi}\cdot\hat{e}(a,x)\bigr)\quad\text{and}\quad\operatorname{sgn}\bigl(\xi\cdot\dot{y}(a)\bigr)\operatorname{sgn}\bigl(\xi\cdot e(a,x)\bigr)=1. \tag{3.16}$$

II.1.b. If $c>s_2(a,x)$, then $L(x,\xi)$ passes between $L(a,x)$ and L_0'. Consequently,

$$\operatorname{sgn}\bigl(\hat{\xi}\cdot\dot{y}(a)\bigr)=-\operatorname{sgn}\bigl(\hat{\xi}\cdot\hat{e}(a,x)\bigr)\quad\text{and}\quad\operatorname{sgn}\bigl(\xi\cdot\dot{y}(a)\bigr)\operatorname{sgn}\bigl(\xi\cdot e(a,x)\bigr)=-1. \tag{3.17}$$

The case $c=s_2(a,x)$ need not be considered because this leads to

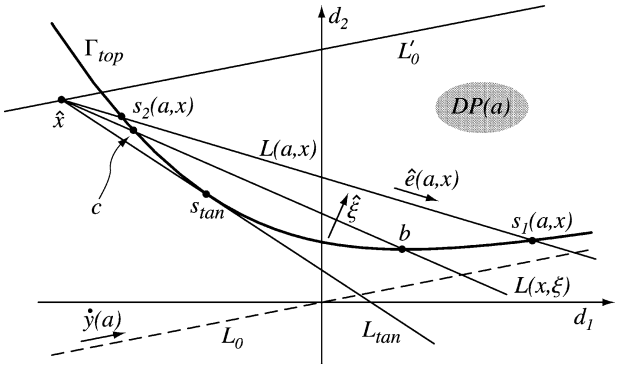

Fig. 3. Top half of the detector plane projected from $y(a)$.

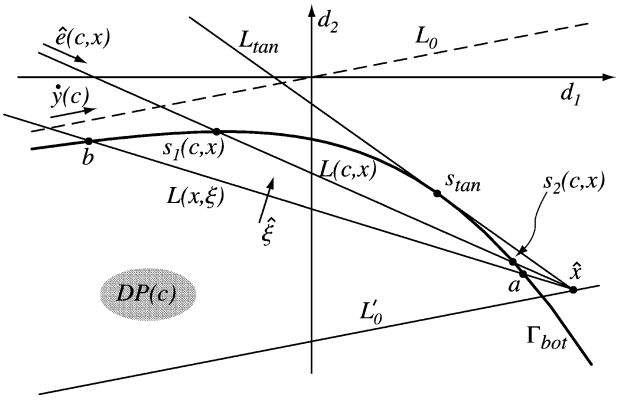

Fig. 4. Correct location of the line $L(x,\xi)$, which is compatible with case II.1.a. Bottom half of the detector plane is shown.

$$\{y(s_0), y(s_2), y(s_1(s_0,s_2))\} \in \Pi(x,\xi), \tag{3.18}$$

which contradicts the assumption $\xi \notin \Xi_\psi(x)$.

II.2. Consider the detector plane $DP(b)$. Since $y(b)$ is the middle point of intersection, $L(x,\xi)$ passes through D_3 because it has to intersect both Γ_{top} and Γ_{bot} at $s=c$, $b<c<s_t(x)$, and $s=a$, $s_b(x)<a<b$, respectively. Therefore,

$$\operatorname{sgn}(\hat{\xi}\cdot\dot{y}(b)) = \operatorname{sgn}(\hat{\xi}\cdot\hat{e}(b,x)) \quad \text{and} \quad \operatorname{sgn}(\xi\cdot\dot{y}(b))\operatorname{sgn}(\xi\cdot e(b,x)) = 1. \tag{3.19}$$

II.3. Consider the detector plane $DP(c)$. Since $y(c)$ is the highest point of intersection and there are two more points in $\Pi(x,\xi)\cap C_{\text{PI}}(x)$, $L(x,\xi)$ intersects the part of Γ_{bot} corresponding to $s_b(x)<s<c$ at two points.

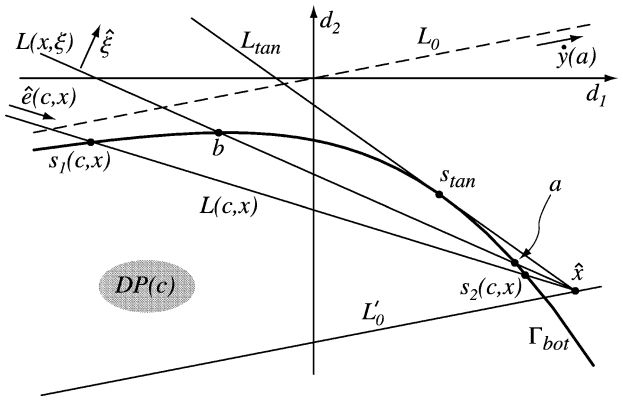

Fig. 5. The arrangement of lines shown here is incompatible with case II.1.a. Bottom half of the detector plane is shown.

II.3.a. Suppose the triple $\{a, b, c\}$ is such that case II.1.a occurs. This implies that $L(x, \xi)$ in the $DP(c)$-plane is between $L(c, x)$ and L_0' as shown in Fig. 4. Indeed, otherwise we get (see Fig. 5):

$$s_2' < a < b < s_1' = \psi\big(c - s_2'\big) + s_2', \quad s_2' := s_2(c). \tag{3.20}$$

Case II.1.a occurs if

$$s_1 = a + \psi(s_2 - a) < b < c < s_2, \quad s_2 := s_2(a). \tag{3.21}$$

From (3.20), (3.21),

$$a + \psi(s_2 - a) < \psi\big(c - s_2'\big) + s_2', \quad s_2' < a < c < s_2. \tag{3.22}$$

Since $0 < \psi' < 1$,

$$a + \psi(s_2 - a) > s_2' + \psi\big(s_2 - s_2'\big) > s_2' + \psi\big(c - s_2'\big), \tag{3.23}$$

and this contradicts (3.22). Therefore,

$$\operatorname{sgn}\big(\hat{\xi} \cdot \dot{y}(c)\big) = -\operatorname{sgn}\big(\hat{\xi} \cdot \hat{e}(c, x)\big) \quad \text{and} \quad \operatorname{sgn}\big(\xi \cdot \dot{y}(c)\big) \operatorname{sgn}\big(\xi \cdot e(c, x)\big) = -1. \tag{3.24}$$

II.3.b. Suppose the triple $\{a, b, c\}$ is such that the case II.1.b occurs. Analogously, this implies that the image of $L(x, \xi)$ in the $DP(c)$-plane is between $L(c, x)$ and $L_{\tan}$ and

$$\operatorname{sgn}\big(\hat{\xi} \cdot \dot{y}(c)\big) = \operatorname{sgn}\big(\hat{\xi} \cdot \hat{e}(c, x)\big) \quad \text{and} \quad \operatorname{sgn}\big(\xi \cdot \dot{y}(c)\big) \operatorname{sgn}\big(\xi \cdot e(c, x)\big) = 1. \tag{3.25}$$

Let us now summarize. If $\xi \in \Xi_1(x)$, $B(x, \xi) = 1$ from (3.15). If $\xi \in \Xi_3(x) \setminus \Xi_\psi(x)$, there are three points of intersection: $s_b(x) < a < b < c < s_t(x)$. Contribution of the

middle point $y(b)$ to the sum in (3.3) equals one, and contributions of the points $y(a)$, $y(c)$ cancel each other (see (3.16) and (3.24), (3.17) and (3.25)). Since the sets $\mathrm{Crit}(x)$ and $\Xi_\psi(x)$ have measure zero, the proof is finished.

4. Practical implementation and numerical experiments

In this section we discuss efficient implementations of inversion formulas (2.13) and (2.14). First, we show that $s_2(s,x)$ actually depends only on s and $\beta(s,x)$. Clearly, the equation in (2.12) depends only on $\beta(s,x)$. To see that the condition $s_2 \in I_{\mathrm{PI}}(x)$ actually depends only on $\beta(s,x)$ an extra argument is required. Let s be fixed, and $\Pi(s,x) := \Pi(s,s_2(s,x))$ be the plane through x, which is found by solving (2.12). By construction, $\Pi(s,x)$ intersects $C_{\mathrm{PI}}(x)$ at three points with parameter values $s, s_1, s_2 \in I_{\mathrm{PI}}(x)$. From (2.5) and (2.6), either $s_2 < s_1 < s$ or $s < s_1 < s_2$, or $s = s_1 = s_2$. Denote $L(s,x) = DP(s) \cap \Pi(s,x)$. By construction, $L(s,x)$ contains $\hat{x}$ and intersects either Γ_{bot} or Γ_{top} at two points s_1 and s_2. The condition $s_1, s_2 \in I_{\mathrm{PI}}(x)$ implies that both intersections occur either on Γ_{bot} to the left of s_b or on Γ_{top} to the right of s_t. Suppose, for example, that $\hat{x}$ is located above L_0, as is shown in Fig. 1. In view of the well-known properties of Γ_{bot}, Γ_{top}, and L_{PI} (see, e.g., [Kat02b]), $s < s_1 < s_2$, that is $L(s,x)$ intersects Γ_{top} at two points. Indeed, if $L(s,x)$ intersected Γ_{bot} at two points, then these points would have been outside $I_{\mathrm{PI}}(x)$. Hence, the slope of $L(s,x)$ is less than the slope of L_0. Pick now any other $x' \in U$, whose projection onto $DP(s)$ coincides with $\hat{x}$. Since $\hat{x}$ is between Γ_{bot} and Γ_{top}, $s \in I_{\mathrm{PI}}(x')$. As before, the slope of $L_{\mathrm{PI}}(x')$ is greater than the slope of L_0, so $s < s_1 < s_2 < s_t(x')$, that is $s_1, s_2 \in I_{\mathrm{PI}}(x')$. Hence, the value $s_2 = s_2(s,x)$ determined for x by solving (2.12) works also for x', and this proves the desired assertion. The case when $\hat{x}$ is below L_0 can be considered analogously.

Consider now (2.13). The preceding argument implies that we can write

$$
\begin{aligned}
u(s,\beta) &:= u\big(s, s_2(s,\beta)\big), \qquad e(s,\beta) := \beta \times u(s,\beta),\ \beta \in S^2,\\
\Psi(s,\beta) &:= \int_0^{2\pi} \frac{\partial}{\partial q} D_f\big(y(q), \cos\gamma\beta + \sin\gamma e(s,\beta)\big)\Big|_{q=s} \frac{1}{\sin\gamma}\,\mathrm{d}\gamma,\\
f(x) &:= -\frac{1}{2\pi^2} \int\limits_{I_{\mathrm{PI}}(x)} \frac{1}{|x - y(s)|} \Psi\big(s, \beta(s,x)\big)\,\mathrm{d}s.
\end{aligned} \tag{4.1}
$$

Fix $s_2 \in [s - 2\pi + \Delta, s + 2\pi - \Delta]$, $s_2 \neq s$, and let $\Pi(s_2)$ denote the plane through $y(s)$, $y(s_2)$, and $y(s_1(s,s_2))$. If $s_2 = s$, $\Pi(s_2)$ is determined by continuity and coincides with the plane through $y(s)$ and parallel to $\dot{y}(s)$, $\ddot{y}(s)$. The family of lines $L(s_2)$ obtained by intersecting $\Pi(s_2)$ with the detector plane is shown in Fig. 6.

By construction, given any $x \in U$ with $\beta(s,x)$ parallel to $\Pi(s_2)$, s_2 used here is the same as s_2 found by solving (2.12). More precisely, the discussion at the beginning of this section gives the following rule for choosing $s_2 = s_2(s,x)$ or, equivalently, the line $L(s_2)$. The first condition is, obviously, $\hat{x} \in L(s_2)$. However, such $L(s_2)$ is not unique. If $\hat{x}$ is

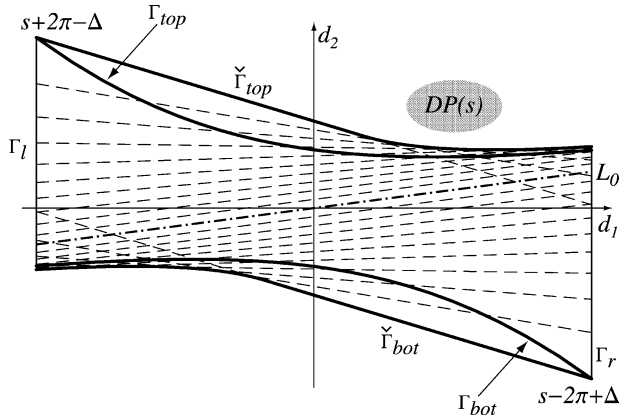

Fig. 6. Dashed segments are segments of lines $L(s_2)$ located between Γ_l and Γ_r. L_0, which also belongs to the family, is shown as a dot-dashed line.

above L_0, we choose $L(s_2)$ so that the two intersections of $L(s_2)$ with Γ_{top} are to the right of $\hat{x}$. If $\hat{x}$ is below L_0, we choose $L(s_2)$ so that the two intersections of $L(s_2)$ with Γ_{bot} are to the left of $\hat{x}$. If $\hat{x} \in L_0$, then $L(s_2) = L_0$, that is $s_2 = s$. This condition assures $s_2 \in I_{\text{PI}}(x)$ and determines $s_2 = s_2(s, x)$ uniquely. Since $e(s, \beta) \cdot \beta = 0$, $|e(s, \beta)| = 1$, we can write (with abuse of notation)

$$\beta = (\cos\theta, \sin\theta), \quad e(s, \beta) = (-\sin\theta, \cos\theta), \quad \beta, e(s, \beta) \in \Pi(s_2). \tag{4.2}$$

Therefore,

$$\Psi(s, \beta) = \int_0^{2\pi} \frac{\partial}{\partial q} D_f\big(y(q), \big(\cos(\theta + \gamma), \sin(\theta + \gamma)\big)\big)\Big|_{q=s} \frac{1}{\sin\gamma}\, \mathrm{d}\gamma, \quad \beta \in \Pi(s_2). \tag{4.3}$$

Equation (4.3) is of convolution type and one application of Fast Fourier Transform (FFT) gives values of $\Psi(s, \beta)$ for all $\beta \in \Pi(s_2)$ at once.

Equations (4.1) and (4.3) imply that the resulting algorithm is of the FBP type. First, one computes shift-invariant filtering of a derivative of cone beam projections using (4.3) for all $s_2 \in [s - 2\pi + \Delta, s + 2\pi - \Delta]$. The second step is backprojection according to (4.1). Since $\partial/\partial q$ in (4.1) and (4.3) is a local operation, each cone beam projection is stored in memory as soon as it has been acquired for a short period of time for computing this derivative at a few nearby points and is never used later.

Comparing (2.13) and (2.14) we see that (2.14) admits absolutely analogous FBP implementation. Moreover, since no derivative along the spiral is present, there is never a need to keep more than one cone beam projection in computer memory at a time.

Consider now the requirements on the detector array imposed by the algorithm. Clearly, they depend on the function ψ in (2.6). In the experiments described below $\psi(t) = t/2$

and $s_1(s_0, s_2)$ is given by (2.8). From the discussion preceding (4.2) we conclude that given any line $L(s_2)$, $s_2 \in [s - 2\pi + \Delta, s + 2\pi - \Delta]$, its segment located between Γ_l and Γ_r should be inside the detector array. These segments are shown in Fig. 6. Thus, the left and right boundaries of the required detector array are still Γ_l and Γ_r, but the new top and bottom boundaries are determined using the envelopes of the lines $L(s_2)$. In Fig. 6 these boundaries are denoted $\check{\Gamma}_{\text{top}}$ and $\check{\Gamma}_{\text{bot}}$. As is seen, the detector array required for the algorithm (its area is denoted A_{alg}) is not much greater than the theoretically minimum one. The latter is bounded by Γ_{top} and Γ_{bot} and its area is denoted A_{min}. The ratio of the areas $A_{\text{alg}}/A_{\text{min}}$ grows as $r/R \to 1$, but slowly. For example, $A_{\text{alg}}/A_{\text{min}} = 1.209$, 1.230, and 1.255 when $r/R = 0.5$, 0.6, and 0.7, respectively. The case $r/R = 0.7$ is shown in Fig. 6. For comparison note that if $r/R = 0.5$ the algorithm of [Kat01,Kat02b] requires a detector array with area $1.93\, A_{\text{min}}$.

Consider $L(s_2)$ corresponding to the largest possible value $s_2 = s + 2\pi - \Delta$ (cf. Fig. 6). Since $s_1 = (s + s_2)/2 = s + \pi - \Delta/2 < s + \pi$, this line intersects Γ_{top} to the right of the d_2-axis and, therefore, intersects Γ_r above the point corresponding to $s_2 = s - 2\pi + \Delta$. Hence, the entire segment of this line located between Γ_l and Γ_r is inside the detector array and

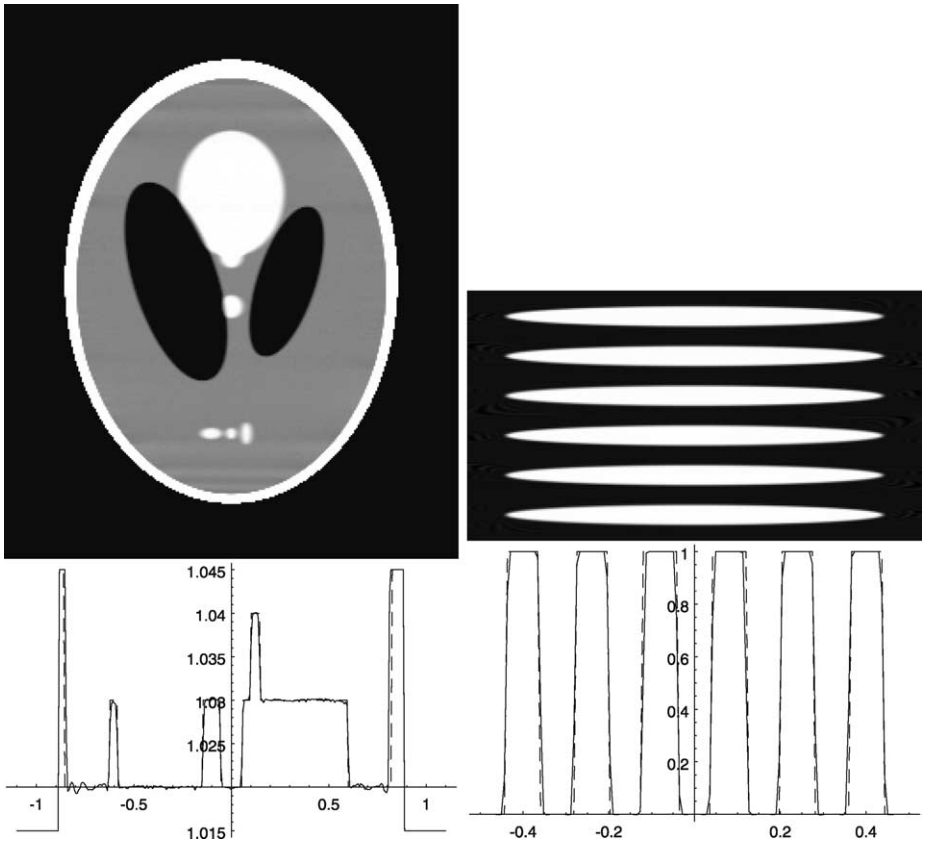

Fig. 7. Experiment 1: Reconstruction formula (2.13), $h = 0.5$.

there is no restriction on how big the cylinder U can be inside the spiral as long as $r/R < 1$. This contrasts with the inversion algorithm of [Kat02b]. In the earlier algorithm one has to know the cone beam data along all the lines tangent to Γ_{top} and Γ_{bot} at points between Γ_l and Γ_r. Therefore, if r/R is close to one (Δ is close to zero), the line tangent to Γ_{top}

Table 1
Parameters of the data collection protocols

Experiment number	1	2	3
R (radius of the spiral)		3	
h (pitch of the spiral)	0.5	0.5	1.0
Axial span of the detector array	0.70	0.72	1.44
Transverse span of the detector array		4.26	
Number of detector rows	50	50	200
Number of detectors per row		500	
Number of source positions per one turn of the spiral	1500	1000	1000

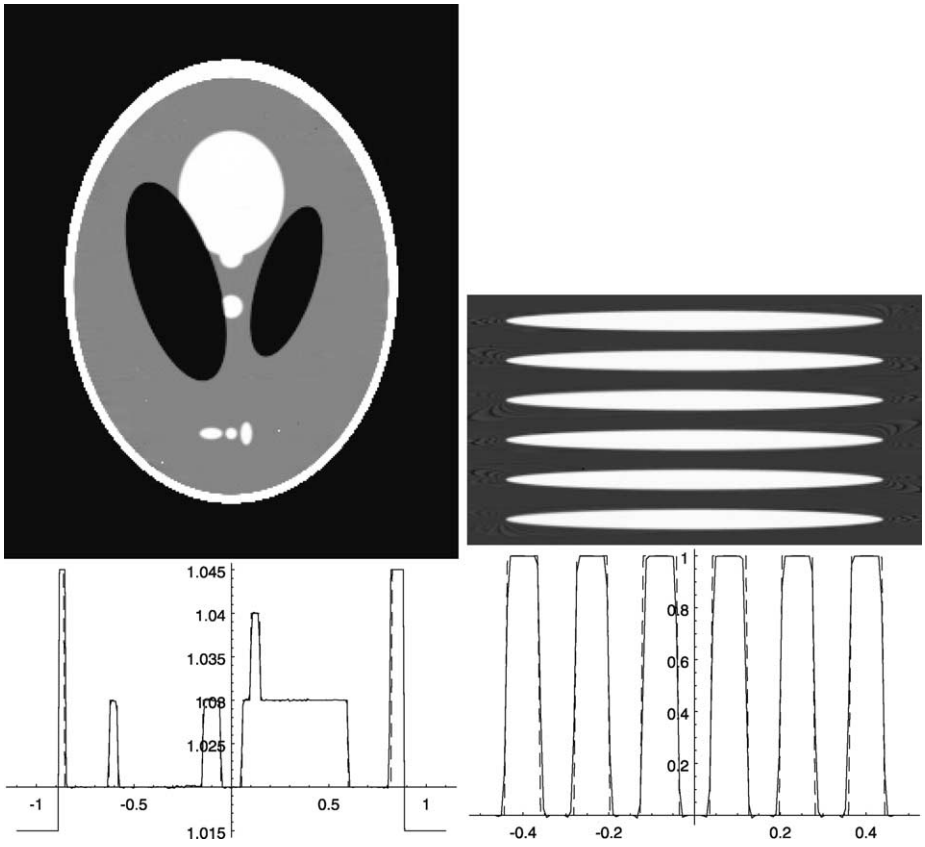

Fig. 8. Experiment 2: Reconstruction formula (2.14), $h = 0.5$.

at $s_{\tan} = s + 2\pi - \Delta$ intersects Γ_r below the point corresponding to $s - 2\pi + \Delta$, thereby increasing significantly the required detector array.

Consider now three numerical experiments. Parameters of the data collection protocols are given in Table 1. Reconstructions in Experiment 1 are done using (2.13), and reconstructions in Experiments 2 and 3 are done using (2.14). The axial span of the detector array in Experiment 2 is slightly bigger than that in Experiment 1 (despite h being equal in both cases) because to use (2.14) we need a little extra space for computing derivatives of the data with respect to the angular variables.

Results of Experiments 1, 2, and 3 are shown in Figs. 7–9, respectively. Left panels of these figures show the 3-D low contrast Shepp phantom (see [KMS98, Table 1] or in [Kat02b, Table 2]). Top half demonstrates a vertical slice through the reconstructed image at $x_1 = -0.25$, and bottom half—the graphs of exact (dashed line) and computed (solid line) values of f along a vertical line $x_1 = -0.25$, $x_2 = 0$. We used the gray scale window $[1.01, 1.03]$ to make low-contrast features visible. Right panels of these figures show the disk phantom, which consists of six identical flattened ellipsoids (lengths of half-axes: 0.75, 0.75, and 0.04, distance between centers of neighboring ellipsoids: 0.16).

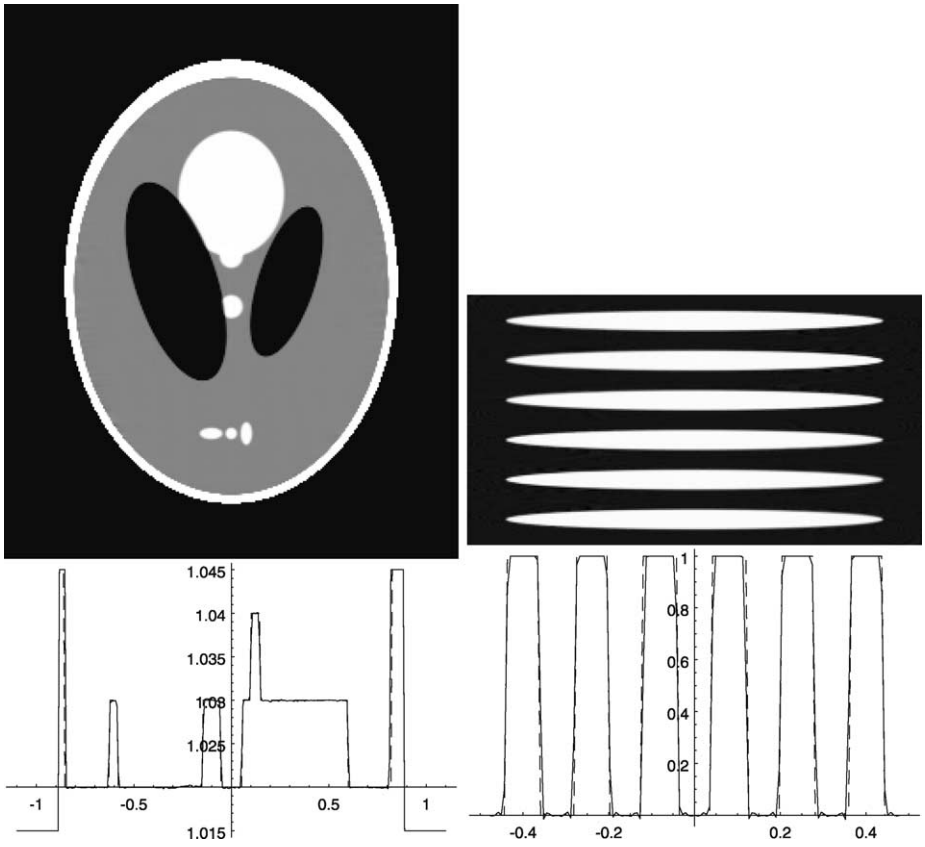

Fig. 9. Experiment 3: Reconstruction formula (2.14), $h = 1.0$.

Again, top half demonstrates a vertical slice through the reconstructed image at $x_1 = 0$, and the bottom half—the graphs of exact (dashed line) and computed (solid line) values of f along a vertical line $x_1 = 0$, $x_2 = 0$.

References

[D+97] P.E. Danielsson et al., Towards exact reconstruction for helical cone-beam scanning of long objects. A new detector arrangement and a new completeness condition, in: D.W. Townsend, P.E. Kinahan (Eds.), Proc. 1997 Meeting on Fully 3D Image Reconstruction in Radiology and Nuclear Medicine, Pittsburgh, 1997, pp. 141–144.

[DNK00] M. Defrise, F. Noo, H. Kudo, A solution to the long-object problem in helical cone-beam tomography, Phys. Med. Biol. 45 (2000) 623–643.

[Kat01] A. Katsevich, An inversion algorithm for Spiral CT, in: A.I. Zayed (Ed.), Proceedings of the 2001 International Conference on Sampling Theory and Applications, May 13–17, 2001, Univ. of Central Florida, 2001, pp. 261–265.

[Kat02a] A. Katsevich, Analysis of an exact inversion algorithm for spiral cone-beam CT, Phys. Med. Biol. 47 (2002) 2583–2598.

[Kat02b] A. Katsevich, Theoretically exact filtered backprojection-type inversion algorithm for Spiral CT, SIAM J. Appl. Math. 62 (2002) 2012–2026.

[KMS98] H. Kudo, N. Miyagi, T. Saito, A new approach to exact cone-beam reconstruction without Radon transform, in: 1998 IEEE Nuclear Science Symposium Conference Record, IEEE, 1998, pp. 1636–1643.